Original Research

Aldh1a1 and *Scl25a30* in diaphragmatic dysfunction

Dong Zhang[1], Wenyan Hao[2], Xujiong Li[3], Pengyong Han[4] and Qi Niu[1]

[1]Department of Critical Care Medicine, Heping Hospital Affiliated to Changzhi Medical College, Changzhi 046000, China; [2]Department of Biomedical Engineering, Changzhi Medical College, Changzhi 046000, China; [3]Department of Physiology, Changzhi Medical College, Changzhi 046000, China; [4]The Central Lab, Changzhi Medical College, Changzhi 046000, China
Corresponding author: Dong Zhang. Email: zhangdongshanxi@126.com

Impact Statement

Mechanical ventilation can cause diaphragmatic weakness and atrophy, which is termed ventilator-induced diaphragmatic dysfunction (VIDD). Transvenous phrenic nerve stimulation (PNS) has been shown to prevent VIDD. Our study gives new insights into the molecular mechanisms by which PNS prevents VIDD and shows for the first time the involvement of two key genes, *Aldh1a1* and *Scl25a30*, which regulate oxidative stress. ALDH1A1 and SCL25A30 protein levels might be useful biomarkers to guide the dose and frequency of electrical stimulation and evaluate the effectiveness of PNS in the prevention of VIDD. SCL25A30 transports sulfate and thiosulfate across the inner mitochondrial membrane and thereby modulates the level of hydrogen sulfide (H_2S). We speculate that H_2S is an important gaseous signaling molecule involved in the mechanism by which electrical stimulation protects diaphragmatic function during mechanical ventilation. H_2S-modifying therapies might be promising approaches for the prevention and treatment of VIDD.

Abstract

New methods to prevent ventilator-induced diaphragmatic dysfunction (VIDD) are urgently needed, and the cellular basis of VIDD is poorly understood. This study evaluated whether transvenous phrenic nerve stimulation (PNS) could prevent VIDD in rabbits undergoing mechanical ventilation (MV) and explored whether oxidative stress-related genes might be candidate molecular markers for VIDD. Twenty-four adult male New Zealand white rabbits were allocated to control, MV, and PNS groups ($n = 8$ in each group). Rabbits in the MV and PNS groups underwent MV for 24 h. Intermittent bilateral transvenous PNS was performed in rabbits in the PNS group. Transdiaphragmatic pressure was recorded using balloon catheters. The diameters and cross-sectional areas (CSAs) of types I and II diaphragmatic fibers were measured using immunohistochemistry (IHC) techniques. Genes associated with VIDD were identified by RNA sequencing (RNA-seq), differentially expressed gene (DEG) analysis, and weighted gene co-expression network analysis (WGCNA). Reverse transcription polymerase chain reaction (RT-PCR), Western blotting, and IHC analyses were carried out to verify the transcriptome profile. Pdi_{60Hz}, Pdi_{80Hz}, and Pdi_{100Hz} were significantly higher in the PNS group than in the MV group at 12 and 24 h ($P < 0.05$ at both time points). The diameters and CSAs of types I (slow-twitch) and II (fast-twitch) fibers were significantly larger in the PNS group than in the MV group ($P < 0.05$). RNA-seq, RT-PCR, Western blotting, and IHC experiments identified two candidate genes associated with VIDD: *Aldh1a1* and *Scl25a30*. The MV group had significantly higher mRNA and protein expressions of *Aldh1a1*/ALDH1A1 and significantly lower mRNA and protein expressions of *Scl25a30*/SCL25A30 than the control or PNS groups ($P < 0.05$). We have identified two candidate genes involved in the prevention of VIDD by transvenous PNS. These two key genes may provide a theoretical basis for targeted therapy against VIDD.

Keywords: Phrenic nerve electrical stimulation, ventilator-induced diaphragmatic dysfunction, prevention, oxidative stress, ALDH1A1, SCL25A30

***Experimental Biology and Medicine* 2022; 247: 1013–1029. DOI: 10.1177/15353702221085201**

Introduction

Invasive mechanical ventilation (MV) is a potentially lifesaving therapy in acutely ill, hospitalized patients.[1] On the basis of a number of scholars' researches, 60–80% of critically ill patients undergoing MV develop ventilator-induced diaphragmatic dysfunction (VIDD),[2,3] and this would be accompanied by the early-onset of progression of the illness in diaphragmatic force-generating capacity.[4] Studies in human donors have indicated that VIDD is related to diaphragmatic injury and atrophy of both slow- and fast-twitch muscle fibers.[5] Furthermore, diaphragmatic atrophy was observed to occur rapidly in cases which had undergone MV, with the muscle thickness decreasing by 9% after only 1 day of MV.[6] As a noticeable challenge, dysfunction of the diaphragm degrades a patient's ability to wean from MV and thus is associated with a poor prognosis.[7,8] Therefore, an effective method of preventing VIDD in patients undergoing MV is urgently needed.

Previous studies have investigated various strategies for the prevention or management of VIDD in cases with critical illness, including pharmacologic approaches, diaphragm-protective ventilation strategies and inspiratory muscle

Copyright © 2022 by the Society for Experimental Biology and Medicine

training (IMT).[9–11] However, none of these strategies have become accepted as standard preventive or therapeutic treatments for VIDD. By contrast, transvenous phrenic nerve stimulation (PNS) is a safe and tolerable method for conditioning the diaphragm for cases in the intensive care unit. A previous study demonstrated that transvenous PNS could be used to treat central sleep apnea in patients with heart failure,[12] confirming the feasibility of using this technique in the clinical setting. However, data are very limited regarding the possible utility of transvenous PNS in the management of VIDD.

Although there have been great improvements in the diagnosis and treatment of VIDD, it is extremely vital to find out the VIDD-associated transcriptome profile. A large body of evidence points to oxidative stress playing a noticeable function in the VIDD-associated pathogenesis.[13–15] The induction of diaphragmatic atrophy via MV would be attributable to the reduction of protein synthesis and elevation of proteolysis, and oxidative stress is essential for the purposes of activating proteases and suppressing protein synthesis in diaphragmatic fibers.[16] Phrenic nerve stimulation (PNS) was noted to improve diaphragmatic contraction, enhance mitochondrial function, reduce oxidative stress, and strengthen diaphragmatic tone.[17] A previous study demonstrated the remarkably upregulation of diaphragmatic *Myog*, *Trim63*, and *Fbxo32*, whereas the noticeably downregulation of *Ppargc1α* was found in the diaphragm in a rat model of controlled MV (CMV).[18] However, no previous studies have identified candidate genes associated with the prevention of VIDD by PNS.

RNA sequencing (RNA-seq) is frequently utilized for the purpose of measuring global gene expression as explained beforehand.[19] Identifying differentially expressed genes (DEGs) is a powerful technique to increase our understanding of the mechanisms of phenotypic variation and gene regulation.[20] However, in the analysis of DEGs, each gene is individually taken into account, and no interaction between genes is assumed. Weighted gene co-expression network analysis (WGCNA) is a method used to characterize the gene expression patterns of multiple samples.[21] It enables the clustering of genes that have similar expression patterns into a module, and it is feasible to investigate the association of the module with the group features. In the present study, we applied RNA-seq, DEG analysis, and WGCNA to rabbits in control, MV, and PNS groups to identify potential key genes involved in the mechanism by which PNS prevents VIDD. We hypothesized that VIDD might be prevented by brief periods of transvenous PNS in the early course of MV and this might be mediated through antioxidant mechanisms. Therefore, the purposes of the current research were to determine whether intermittent transvenous PNS would be protective against VIDD and to find out target genes that might be involved in this process.

Materials and methods

Animals and grouping

We attempted to obtain 24 male adult New Zealand white rabbits (weight, 2.5–3.0 kg) from the Laboratory Animal Research Center of Shanxi Medical University (Taiyuan, China). The rabbits were selected for this study because of their moderate body type and based on studies conducted on the VIDD models of rabbits.[22–24] The animals were housed under a standard alternating 12 h light–dark cycle with food and water provided *ad libitum*. We also followed the Guidelines for the Care and Use of Laboratory Animals to carry out animal experiments. The approval of study was attained from the Institutional Ethics Committee of Changzhi Medical College. All the rabbits were anesthetized with sodium pentobarbital intraperitoneal (i.p.) injection, and then divided into the following three groups on a random basis (Figure 1): control group (anesthetized with i.p. injection only, $n = 8$), MV group (anesthetized with i.p. injection and mechanically ventilated, $n = 8$), and PNS group (anesthetized with i.p. injection and stimulation of the bilateral phrenic nerves for 10 min repeated every 2 h during MV, $n = 8$).

MV

The animal was anesthetized with sodium pentobarbital, which was administered intraperitoneally (40 mg/kg) and then continuously via the right marginal ear vein (15–25 mg/kg). The trachea was connected to the mechanical ventilator (Inspira ASVV 55-7058; Harvard Apparatus, Cambridge, MA, USA) after tracheotomy. The ventilator settings[23] were as follows: inspired fraction of oxygen, 0.40; tidal volume (Vt), 6–8 mL/kg; respiratory rate, 40 cycles per minute; and positive end-expiratory pressure, 2 cm H_2O.[24] The volume-controlled ventilation mode was used to suppress diaphragmatic activity. Rabbits were kept warm with heating pads during the procedure (Figure 2). Arterial blood was obtained every 12 h for determination of PO_2, PCO_2, and pH at 37°C with a blood gas analyzer (Start Profile Critical Care Xpress; Nova Biomedical, Waltham, MA, USA). The animals were euthanized by exsanguination under anesthesia after 24 h of MV. The immediately storage of samples of the diaphragm in liquid nitrogen was undertaken for the subsequent stages of analysis.

Transvenous PNS

The bilateral external jugular veins were isolated in the neck. A 7.0F percutaneous sheath introducer (Arrow, Teleflex, Morrisville, NC, USA) was inserted into each external jugular vein to allow the passage of an electrode catheter for PNS (Medtronic, Minneapolis, MN, USA). While palpating for diaphragmatic contraction, the position of the electrode catheter on each side was adjusted to stimulate the phrenic nerve with the highest efficacy. Once the optimal position had been determined, the electrode catheter was attached firmly to the vein to avoid further displacement. A pulse generator (Department of Biomedical Engineering, Changzhi Medical College, Changzhi, China) was used for bilateral transvenous PNS. The parameters used for electrical stimulation were as follows: frequency, 40 Hz; pulse duration, 300 μs; respiratory rate, 40 per min; contraction/relaxation time, 1:2; peak current, 2.5 mA.

Measurement of the diaphragmatic contractile properties *in vivo*

Transdiaphragmatic pressure (Pdi) was measured[25] during supramaximal stimulation at frequencies of 10, 20, 40, 60, 80, and 100 Hz (train duration, 500 ms; pulse duration, 150 μs; current intensity, 3 mA) applied in a serial manner with 3-min recovery periods between successive stimulus trains at the end of expiration. After recording of at least

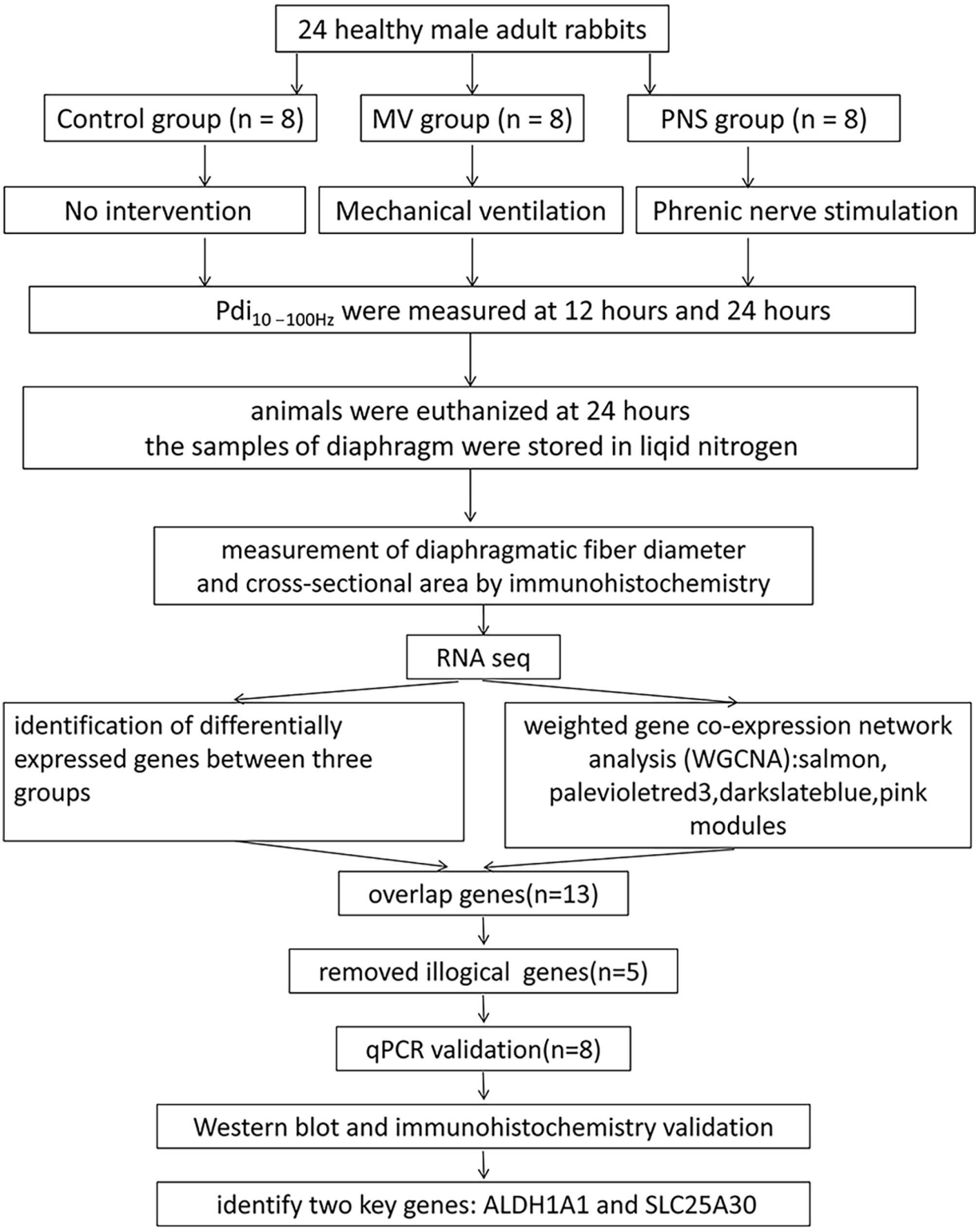

Figure 1. Experimental flowchart.

three consistent Pdi values, their average value was computed for the subsequent stages of analysis.

Histology

Once the animal had been euthanized, a portion of the right costal diaphragm at the mid-axillary line was immediately removed (the same segment was resected for all animals). The muscle tissue was fixed in 4% paraformaldehyde and cut perpendicular to the direction of the muscle fibers into sections no more than 0.3 cm in length. The tissue samples were dehydrated and embedded in paraffin using conventional techniques. The embedded tissue samples were frozen (–20°C) and sectioned to a thickness of 3 μm. Staining with hematoxylin–eosin (HE) was performed in accordance with standard methods.[26]

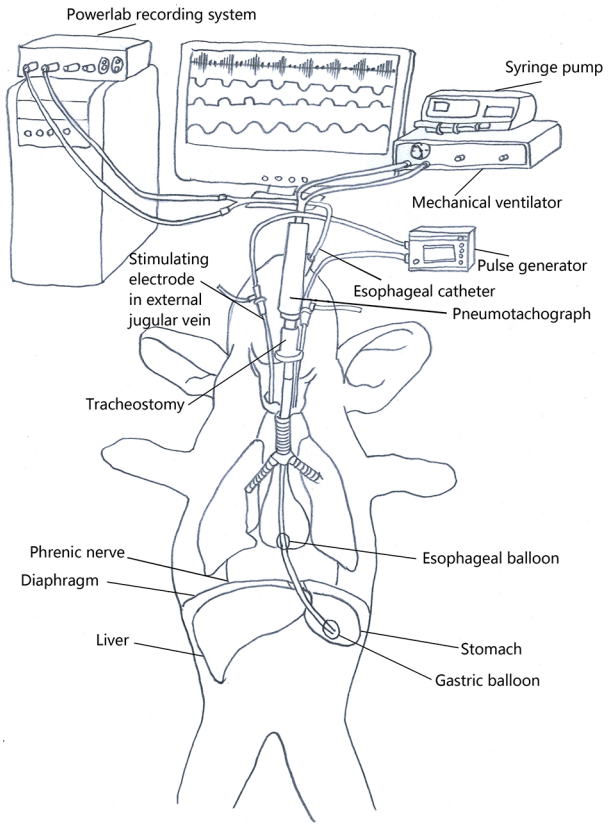

Figure 2. Diagrammatic representation of the experimental setup. The rabbit was placed in the supine position and anesthetized. The endotracheal tube was connected to a mechanical ventilator. The gastric and esophageal balloon catheter was connected to the recording system for the measurement of transdiaphragmatic pressures. The electrical stimulation electrodes were connected to the pulse generator. The computer monitor displayed real-time electrocardiography, airflow, esophageal pressure, and gastric pressure signals.

RNA–seq

We attempted to compare transcriptional differences among the control, MV, and PNS groups via RNA-seq. The extraction of total RNA from diaphragmatic tissues was undertaken through Trizol reagent (15596026; Ambion, Austin, TX, USA) in accordance with instructions provided by manufacturer. Utilization of NanoDrop and Agilent 2100 bioanalyzers (Thermo Fisher Scientific, Waltham, MA, USA) enabled us to carry out the investigation of RNA integrity, and RNA integrity $\geqslant 7$ was taken as a threshold into account for the purpose of analyzing samples. The sequencing of libraries was conducted on an MGISEQ-2000 platform, and data processing was undertaken on the Beijing Genomics Institute (BGI) online server (http://report.bgi.com; Huada Gene Science and Technology Service Co. Ltd, Shenzhen, China). DEG analyses were conducted to investigate the molecular differences among the three groups. The Kyoto Encyclopedia of Genes and Genomes (KEGG) pathway annotation was utilized to classify the metabolic pathways with significant enrichment of the DEGs. Using WGCNA, identification of the modules that were noticeably correlated with the group features was carried out. We could successfully detect the key genes via overlapping the differential genes and the significant core modules (Figure 1).

RT-PCR

Total RNA was isolated using Trizol reagent (15596026; Ambion), and cDNA was synthesized using PrimeScript II RTase (2690A, Takara Bio USA, San Jose, CA, USA), recombinant RNase inhibitor (2313A, Takara Bio USA), and oligo (dT) 18 primer (3806, Takara Bio USA). The polymerase chain reaction (PCR) mixtures were prepared to a final volume of 20 µL using SYBR FAST qPCR Master Mix (KM4101, Kapa Biosystems, Woburn, MA, USA). Reverse transcription polymerase chain reaction (RT-PCR) was undertaken via a CFX-Connect 96RT PCR detection system (Bio-Rad, Hercules, CA, USA). The comparative CT method ($\Delta\Delta$CT) was utilized for the purpose of analyzing gene expression data, and β-actin was regarded as an internal control. The presentation of results was undertaken in form of fold-change relative to control. Primer sequences are listed in Table 1.

Western blotting

We attempted to carry out Western blotting as explained in advance.[27] Briefly, blockage of membranes in 5% milk solution was undertaken, and incubation was implemented with primary antibodies against SLC25A30 (JL-T0287, Jianglai, Shanghai, China), TMPRSS13 (JL-T0294, Jianglai), MAPRE1 (JL-T0287, Jianglai), BDKRB1 (bs-8675R, Bioss, Beijing, China), CST3 (C8950, United States Biological, Salem, MA, USA), MICAL2 (NBP2-83205, Novus Biologicals, Littleton, CO, USA), UCH-L1 (NBP2-29420, Novus), ALDH1A1 (NBP2-15336, Novus), or β-actin (PAB36265, Bioswamp, Wuhan, China) overnight at 4°C. Subsequently, exposure of membranes to goat antirabbit immunoglobulin G (IgG) (SAB43714, Bioswamp) was carried out for 1 h at room temperature. Membranes were scanned and analyzed with Tanon GIS version 4.2 (Tanon Technology, Shanghai, China). The

Table 1. Primer information for RT-PCR.

Gene name	Forward (5′–3′)	Reverse (3′–5′)	Product size (bp)
ALDH1A1	TGGCAGACTTACCTACCCC	GCCTTATCTCCTTCTTCAATCA	157
SLC25A30	CCCTCAACTGGAAGCCGT	CGATCCCCGAGTACAGCG	210
MAPRE3	CATCCTCCGCAAGAACCC	GCTGAAGTAGAAGTCACGCTCC	139
UCH-L1	GTCCCCTGAAGACAGAGCAA	GGCATTCGCCCATCAAG	168
TMPRSS13	CATCATCAACGGCAACTACAC	CGTCTGTCTCCTTGGTCTTG	182
MICAL2	GGCAGTCAGAACAAAGTCAAG	AGAGCACAGGGTGGTCTTAC	129
BDKRB1	TCCAGCCCTCCAACCAGA	GGAAGACGGACAGGACGAA	159
Cystatin C	GGCAGATCGTAAGTGGCG	GTCGTGGAAAGGACAGTTGG	101
β-actin	CCAGGTCATCACCATCGG	TGTCCAGGTCGCACTTCA	131

quantification of density of the bands was undertaken, followed by normalization to the β-actin content.

Immunohistochemistry

We attempted to carry out immunohistochemistry (IHC) for the purpose of analyzing the expression profiles of specific proteins in the diaphragmatic tissue. First, the paraffin-embedded tissue was sectioned to a thickness of 3 μm for IHC, and tissue slide was baked for 30 min at 60°C. Then, xylene was utilized for thrice deparaffinization, 5 min each, and twice rehydration was implemented via 100% ethanol (each round, 3 min); the process was continued by alcohol (95, 70, and 50; each round, 5 min). After rinsing in distilled water, the blockage of endogenous peroxidase activity was undertaken via 10-min incubating tissue slide in 3% H_2O_2 solution in methanol. After completing the several steps on the basis of the instruction provided by manufacturer, it was attempted to incubate the tissue sections with primary antibodies (mouse antifast myosin skeletal heavy chain [ab51263, Abcam, Cambridge, UK], mouse antiALDH1A1 [NBP2-15336, Novus] or mouse antiSLC25A30 [JL-T0287, Jianglai]) overnight at 4°C. Rinsing of slides with phosphate-buffered saline (PBS) was implemented, and this was continued by reacting with goat antirabbit IgG secondary antibody (ab205719, Abcam) for 1 h at 37°C. The hematoxylin was utilized for the purpose of counterstaining tissue slides for 2 min, followed by mounting with a coverslip. Images were captured from randomly selected microscopic fields using a BX41 microscope (Olympus, Tokyo, Japan). Muscle fiber diameter, cross-sectional area (CSA), and integral optical density (IOD) were calculated quantitatively with Image-Pro Plus version 6.0 (Media Cybernetics, Bethesda, MD, USA). The number of diaphragm fibers that could be calculated is between 25 and 35.

Statistical analysis

Processing of data was undertaken via SPSS 22.0 software (IBM, Armonk, NY, USA). The Kolmogorov–Smirnov test was employed for the purpose of testing normal distribution of data, and the presentation of data was in form of mean ± standard deviation (SD). It was attempted to conduct the comparison of differences among multiple groups via one-way analysis of variance (ANOVA) followed by post hoc Tukey's test. A two-tailed $P < 0.05$ denoted the statistical significance.

Results

Comparisons of physiological parameters between the three groups

There were no significant differences between the control, MV, and PNS groups in heart rate, blood pressure, Vt, arterial pH, arterial PO_2, and arterial PCO_2 at baseline (Table 2). Furthermore, no significant differences were detected between groups in any of these parameters at 12 and 24 h (Table 2), indicating that these physiological parameters were not confounding factors for any differences between groups in diaphragmatic pressures or morphology.

Table 2. Comparison of physiological parameters between the three groups at different time points.

	Control group ($n = 8$)			CMV group ($n = 8$)			PNS group ($n = 8$)		
	0 h	12 h	24 h	0 h	12 h	24 h	0 h	12 h	24 h
Vt (mL/kg)	6.91 ± 2.14	5.95 ± 1.96	6.46 ± 1.25	5.98 ± 1.73	7.32 ± 1.40	7.03 ± 1.90	6.80 ± 1.74	7.57 ± 1.83	7.36 ± 2.11
BP (cmH_2O)	115.63 ± 10.01	126.42 ± 11.06	112.90 ± 98.48	122.95 ± 7.00	109.09 ± 7.96	106.78 ± 9.37	123.78 ± 6.08	111.45 ± 10.11	108.80 ± 8.72
HR (/min)	242.07 ± 16.03	239.06 ± 15.09	235.61 ± 12.79	251.12 ± 23.43	233.42 ± 15.98	230.89 ± 22.42	235.15 ± 12.99	238.12 ± 26.70	225.27 ± 19.92
pH	7.43 ± 0.10	7.39 ± 0.05	7.30 ± 0.04	7.33 ± 0.07	7.34 ± 0.06	7.33 ± 0.04	7.35 ± 0.05	7.33 ± 0.06	7.28 ± 0.08
PO_2 (kPa)	134.78 ± 19.48	139.49 ± 15.89	150.45 ± 22.09	142.80 ± 27.70	154.20 ± 35.20	158.00 ± 19.30	123.30 ± 13.60	147.10 ± 26.80	145.00 ± 28.90
PCO_2 (kPa)	29.50 ± 2.56	29.79 ± 2.35	28.00 ± 4.40	28.40 ± 6.10	29.00 ± 6.30	27.80 ± 1.60	27.40 ± 4.50	27.00 ± 7.10	27.10 ± 5.60

CMV: controlled mechanical ventilation; PNS: phrenic nerve electrical stimulation; BP: blood pressure; HR: heart rate; $PaCO_2$: arterial partial pressure of carbon dioxide; PaO_2: arterial partial pressure of oxygen; and Vt: tidal volume

Data are expressed as the mean ± standard deviation.

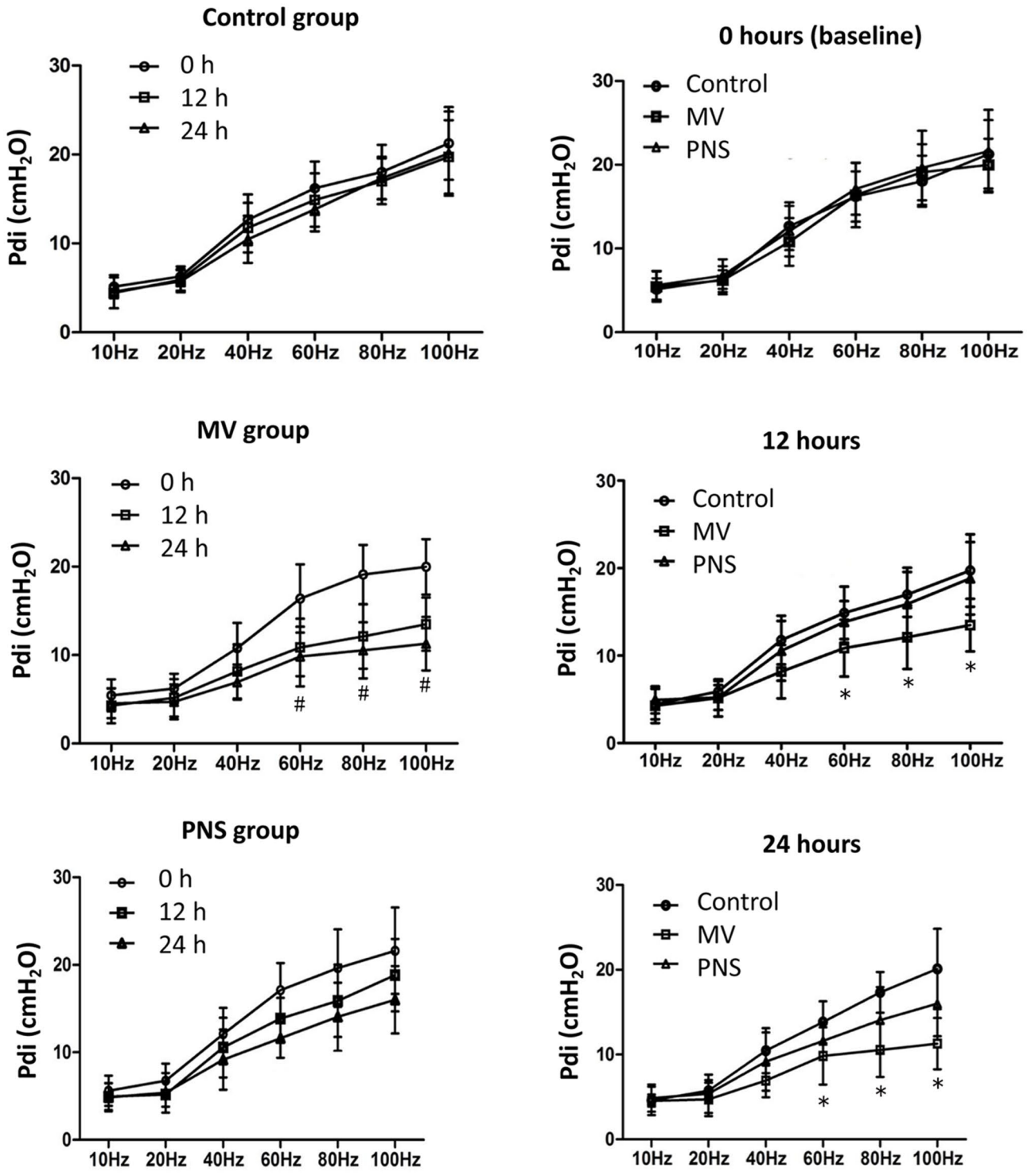

Figure 3. Comparison of diaphragmatic tension–frequency curves between three groups.
Curves showing the relationship between transdiaphragmatic pressure (Pdi) and stimulation frequency were obtained for the control ($n=8$), MV ($n=8$), and PNS ($n=8$) groups at 0, 12, and 24 h. Presentation of data was in form of mean ± SD. *$P<0.05$ versus corresponding value in MV group; #$P<0.05$ versus baseline (0 h) in the same group.

Comparisons of diaphragmatic pressures and the diameters and CSAs of diaphragmatic fibers between the three groups

The Pdi generated during stimulation with frequencies ranging from 10 to 100 Hz showed little or no variation over time in the Control group (Figure 3). However, Pdi_{60Hz}, Pdi_{80Hz}, and Pdi_{100Hz} in the MV group were significantly lower after 12 h of MV ($P<0.05$) and after 24 h of MV ($P<0.05$) than at baseline (Figure 3), and Pdi_{100Hz} at 24 h was only ~56% of its initial baseline value. Pdi during MV was better maintained in the PNS group than in the MV group, with Pdi_{60Hz}, Pdi_{80Hz} and Pdi_{100Hz} significantly higher in the PNS group ($P<0.05$) than in the MV group at both 12 and 24 h (Figure 3).

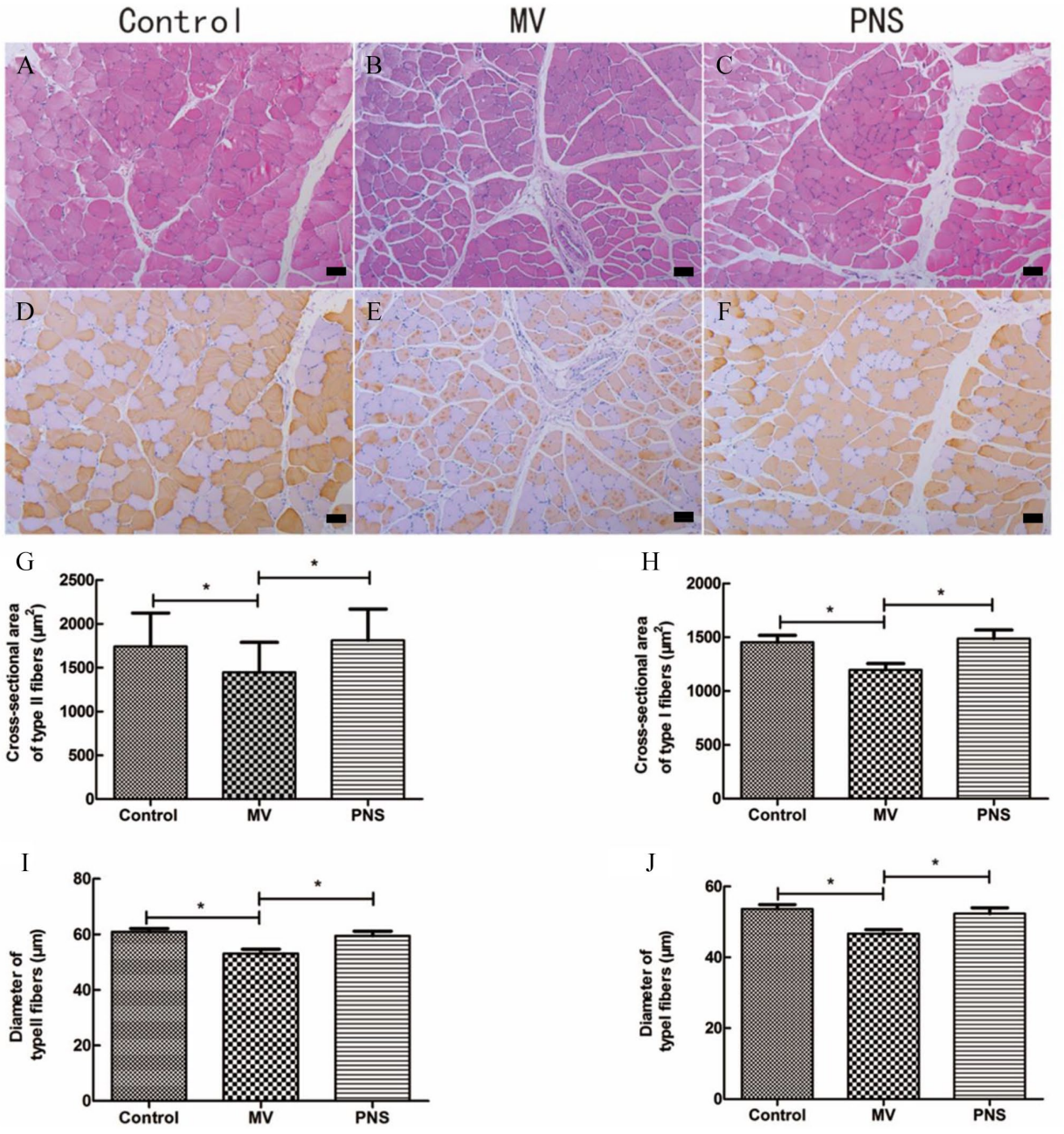

Figure 4. Representative images were obtained using immunohistochemistry and histology techniques. (A to C) Staining with hematoxylin–eosin. Scale bar = 50 μm. (D to F) Immunostaining of antifast myosin skeletal heavy chain. Histology and immunohistochemistry demonstrated the presence of types II (which react with the primary antibody and appear orange-red) and I (which do not react with the antibody and appear off-white) fibers in all three groups as well as morphological differences between the three groups. Scale bar = 50 μm. (G to J) Comparisons of the diameters and cross-sectional areas (CSAs) of types I (slow-twitch) and II (fast-twitch) fibers between the three groups. The diameters and CSAs of the types I and II fibers were significantly smaller in the MV group than in the control or PNS groups. (A color version of this figure is available in the online journal.)
*$P < 0.05$.

In addition, histological (staining with HE) and immunohistochemical evaluations of the diaphragmatic fibers demonstrated morphological differences between the control, MV, and PNS groups (Figure 4(A) to (F)). The diameters and CSAs of types I (slow-twitch) and II (fast-twitch) fibers were significantly smaller in the MV group than in the control or PNS groups ($P < 0.05$; Figure 4(G) to (J)).

Biomedical analyses

We, in the present research, aimed to identify VIDD-associated transcriptome profiles using RNA-seq. In total, 24 samples were included in the differential expression analysis. A total of 3688 genes were significantly differentially expressed in the MV group in comparison to the control group, involving 1945 upregulated and 1734 downregulated genes (Figure 5(A)). Sixty-three genes were significantly differentially expressed in the PNS group in comparison to the MV group, with 24 upregulated and 39 downregulated genes (Figure 5(B)). Twenty-two genes were identified by overlapping the differential expression genes between the MV versus control groups and PNS versus MV groups: *Aldh1a*, *Bdkrb1*, *Cst3*, *Fosl1*, *Dync1i1*, *Slc25a30*, *Camsap3*, *C12h6orf89*, *Smyd2*, *Dsc2*, *Slc38a10*, *Adm*, *Loc100348748*, *Loc100351810*,

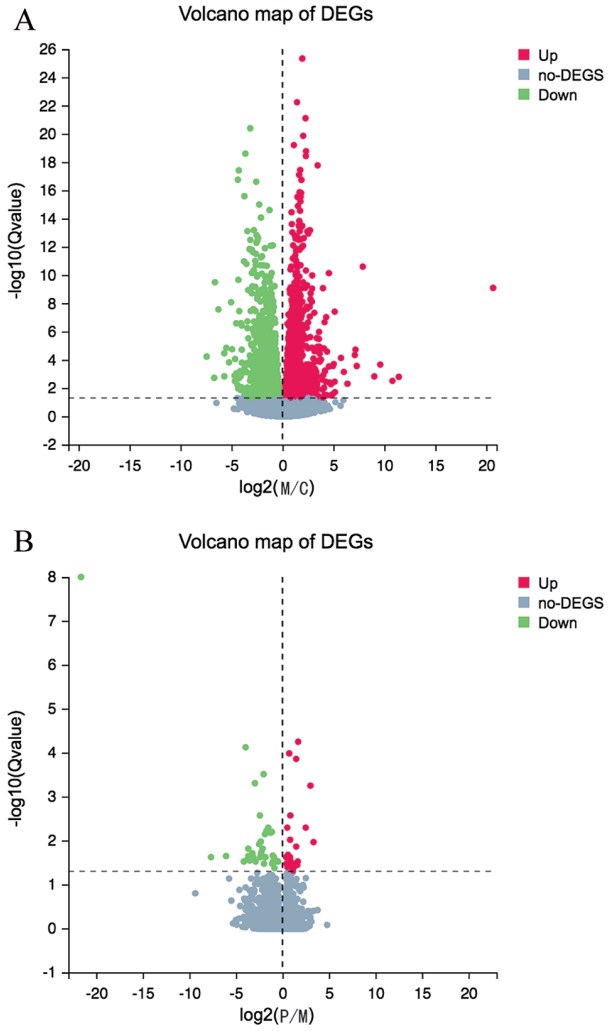

Figure 5. Detection of DEGs. (A) Volcano plot depicting DEGs in the control and MV groups. $\log_2FC > 1$ and false discovery rate (FDR) < 0.05 in vertical and horizontal lines, respectively. (B) Volcano plot depicting DEGs in the PNS and MV groups.$\log_2FC > 1$ and FDR < 0.05 in vertical and horizontal lines, respectively. (A color version of this figure is available in the online journal.)

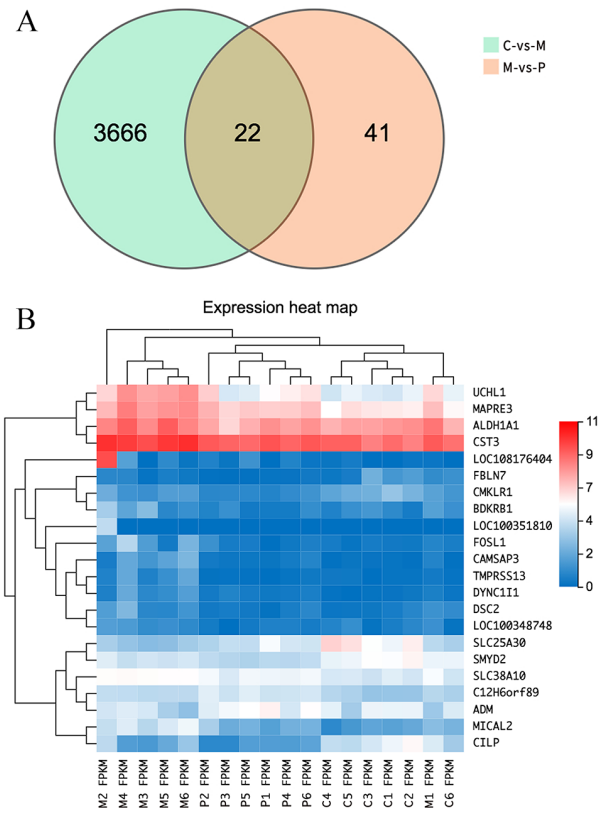

Figure 6. Overlap of differentially expressed genes (DEGs) between groups. (A) Venn diagram depicting the overlap of DEGs in MV versus control groups and PNS versus MV groups. The number of DEGs included 22 up- and downregulated genes. (B) Heat map representing the 22 overlapping DEGs in MV versus control groups and PNS versus MV groups. $\log_2FC < -1$ and $\log_2FC > 1$ are depicted with shades of blue and red, respectively. (A color version of this figure is available in the online journal.)

Mical2, *Fbln7*, *Tmprss13*, *Cmklr1*, *Uchl1*, *Cilp*, *Mapre3*, and *Loc108176404* (Figure 6). WGCNA indicated that the salmon and palevioletred3 modules had positive correlations with the control group, whereas the darkslateblue and pink modules were correlated with the PNS group (Figures 7 and 8). After overlapping the DEGs with the core significant modules and removing five illogical genes, only eight genes (*Slc25a30*, *Tmprss13*, *Mapre1*, *Bdkrb1*, *Cst3*, *Mical2*, *Uchl1*, and *Aldh1a1*) were selected. Pathway enrichment analysis for the DEGs in the control versus MV groups revealed that the ubiquitin proteasome signaling pathway was the most significantly changed pathway (Figure 9(A)), while the fatty acid degradation signaling pathway was identified as the most representative altered canonical pathway for PNS versus MV groups (Figure 9(B)). There were no common canonical pathways between the MV versus control groups and PNS versus MV groups.

Aldh1a1 and Slc25a30

On the basis of RT-PCR results, in comparison with PNS group, fold-changes in *Bdkrb1* and *Cst3* mRNA relative to control did not remarkably differ in the MV group. As confirmed by Western blotting, the expressions of BDKRB1, CST3, TMPRSS13, MAPRE1, MICAL2, or UCH-L1 proteins did not remarkably differ between the MV and PNS groups. However, the RNA-seq (fragments per kilobase of exon per million mapped fragments [FPKM]), RT-PCR (fold-change in mRNA level), Western blotting, and IHC analyses revealed that the MV group had significantly higher *Aldh1a1* expression/ALDH1A1 protein levels ($P < 0.05$; Figure 10) and significantly lower *Slc25a30* expression/SLC25A30 protein levels ($P < 0.05$; Figure 11) than the control or PNS groups.

Discussion

Notable findings of this study are summarized as follows: (1) Pdi_{60Hz}, Pdi_{80Hz}, and Pdi_{100Hz} were significantly higher in the PNS group than in the MV group at 12 and 24 h; (2) the MV group exhibited significant reductions in the diameters and CSAs of types I and II diaphragmatic fibers in comparison with the control or PNS groups; and (3) the MV group had significantly higher mRNA and protein expressions of *Aldh1a1*/ALDH1A1 and significantly lower mRNA and protein expressions of *Slc25a30*/SLC25A30 than the control or PNS groups. Taken together, our data show that transvenous PNS can prevent VIDD in rabbits undergoing MV. In addition, ALDH1A1 and SLC25A3 were identified as candidate molecular targets mediating the effects of PNS to prevent VIDD.

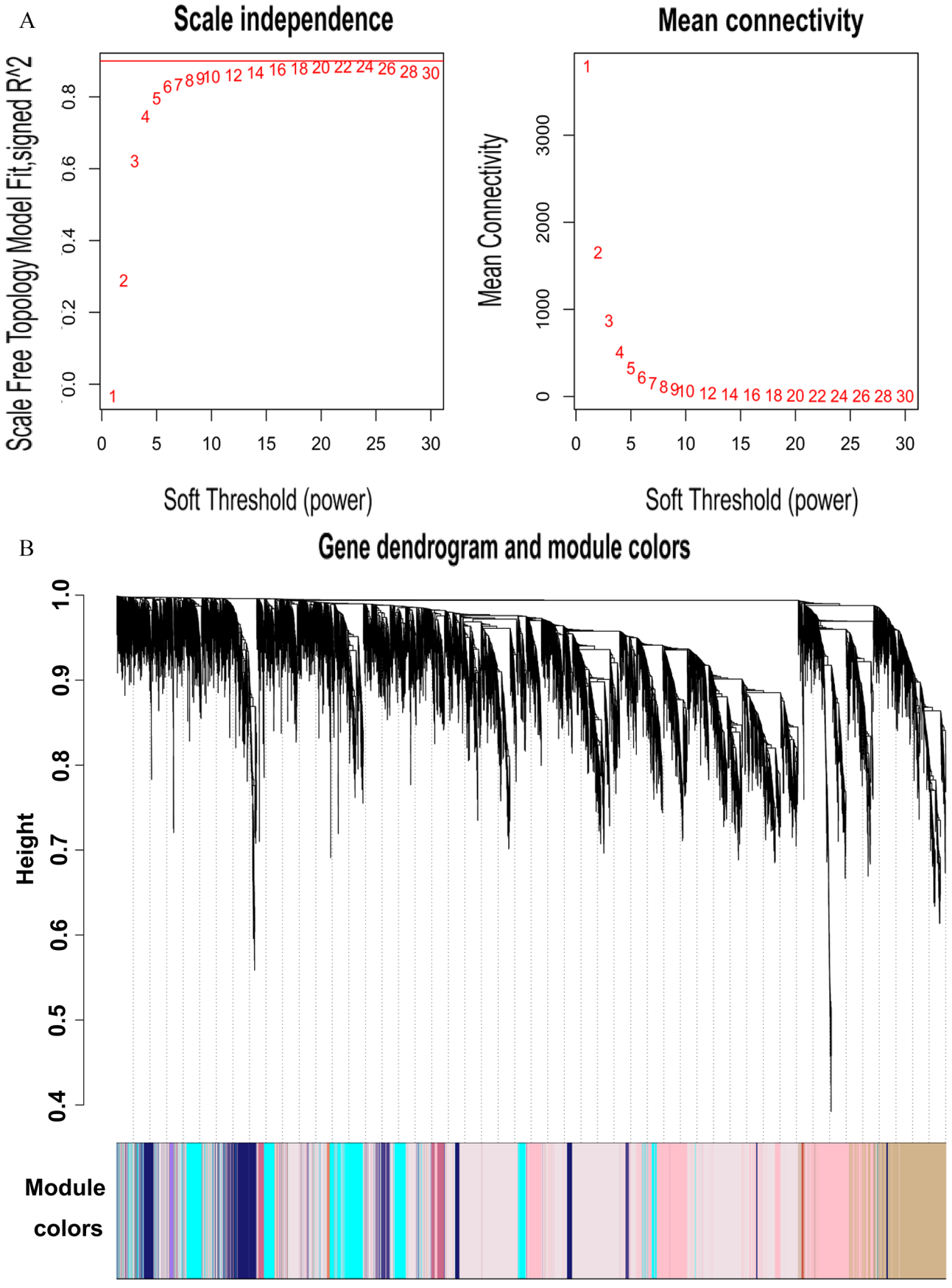

Figure 7. WGCNA. (A) Utilization of diverse soft threshold powers to analyze the scale-free fit index and the mean connectivity. (B) In modules, dendrograms were utilized to present the co-expressed genes. A color-coded module, covering highly connected genes, is represented by a colored row. (A color version of this figure is available in the online journal.)

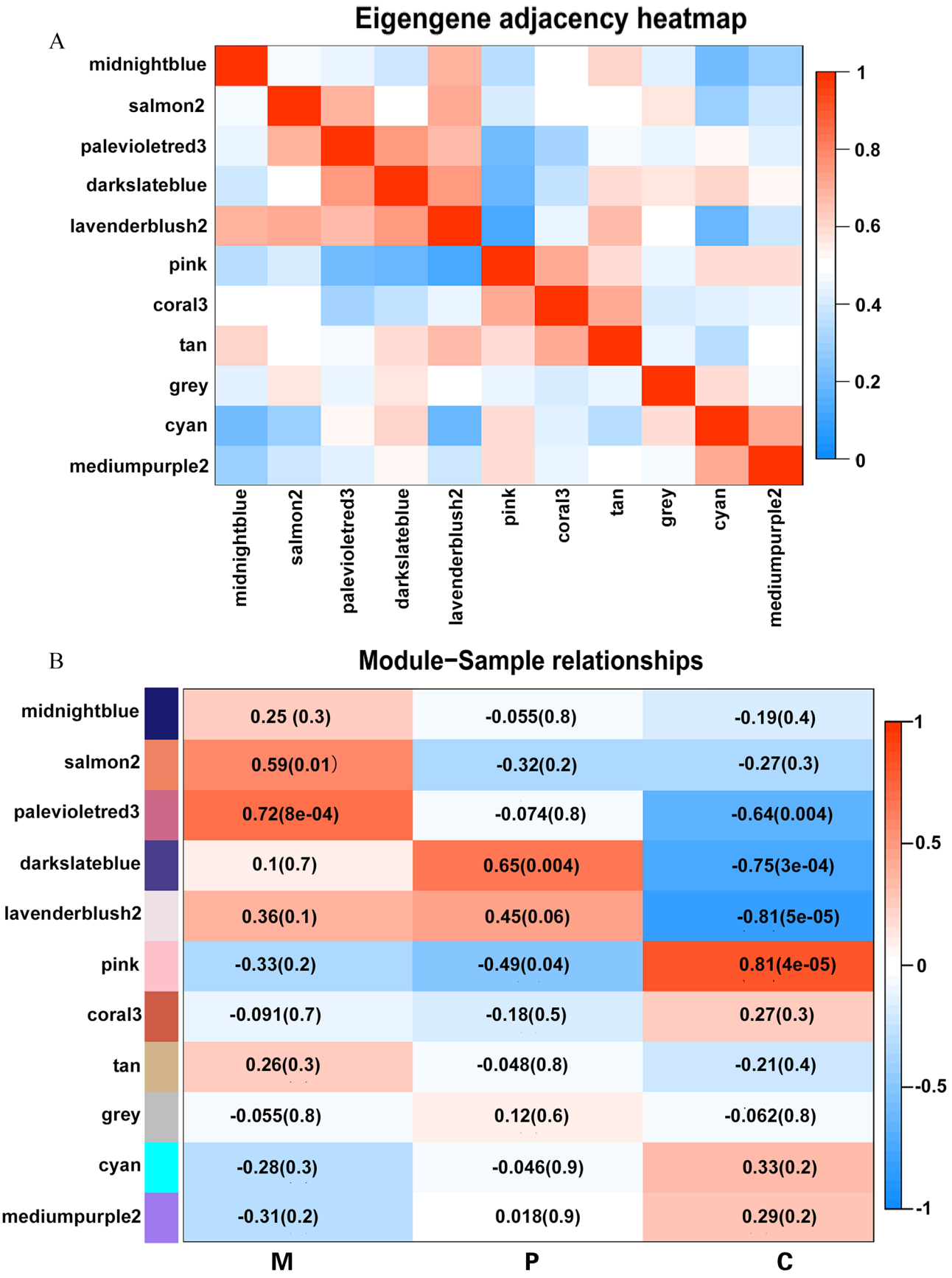

Figure 8. Eigengene heat maps. (A) Heat map of eigengene adjacency. In the heat map, a colored module eigengene is associated with a row/column. Low (negative correlation) and high (positive correlation) adjacencies are marked with blue and red, respectively. (B) Heat map of the correlation between the module eigengenes and the group features. A module eigengene and a group feature are associated with a row and a column, respectively. The corresponding *P* value and correlation are involved in each cell. The selection of four modules (salmon, palevioletred3, pink, and darkslateblue), as the key modules, for further analysis based on the module significance value and the correlation coefficient. (A color version of this figure is available in the online journal.)

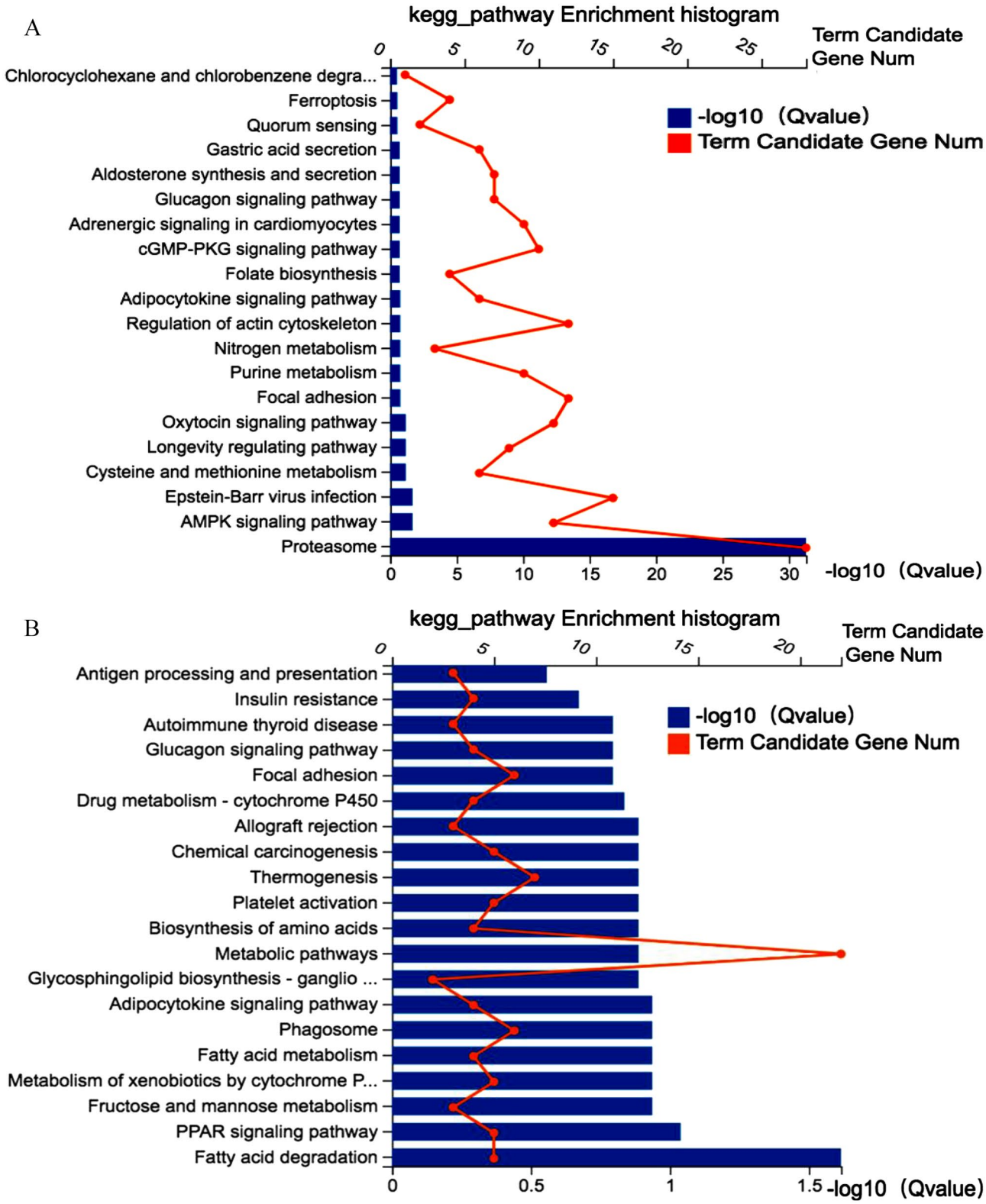

Figure 9. KEGG pathway annotation analysis. (A) Ubiquitin proteasome signaling pathway was the most significantly changed pathway for control versus MV groups. (B) Fatty acid degradation signaling pathway was the most significantly changed pathway for PNS versus MV groups. (A color version of this figure is available in the online journal.)

Association of VIDD with histobiochemical signs of diaphragmatic injury and atrophy, as well as a prompt loss of diaphragmatic force-generating capacity has been confirmed. Our study revealed that the Pdi_{100Hz} had decreased to 56% of the baseline value after 1 day of MV, which is similar to the value of 63% reported by Sassoon.[23] Significant differences could be detected in the mean diameters and CSAs of types I and II diaphragmatic fibers among the three groups.

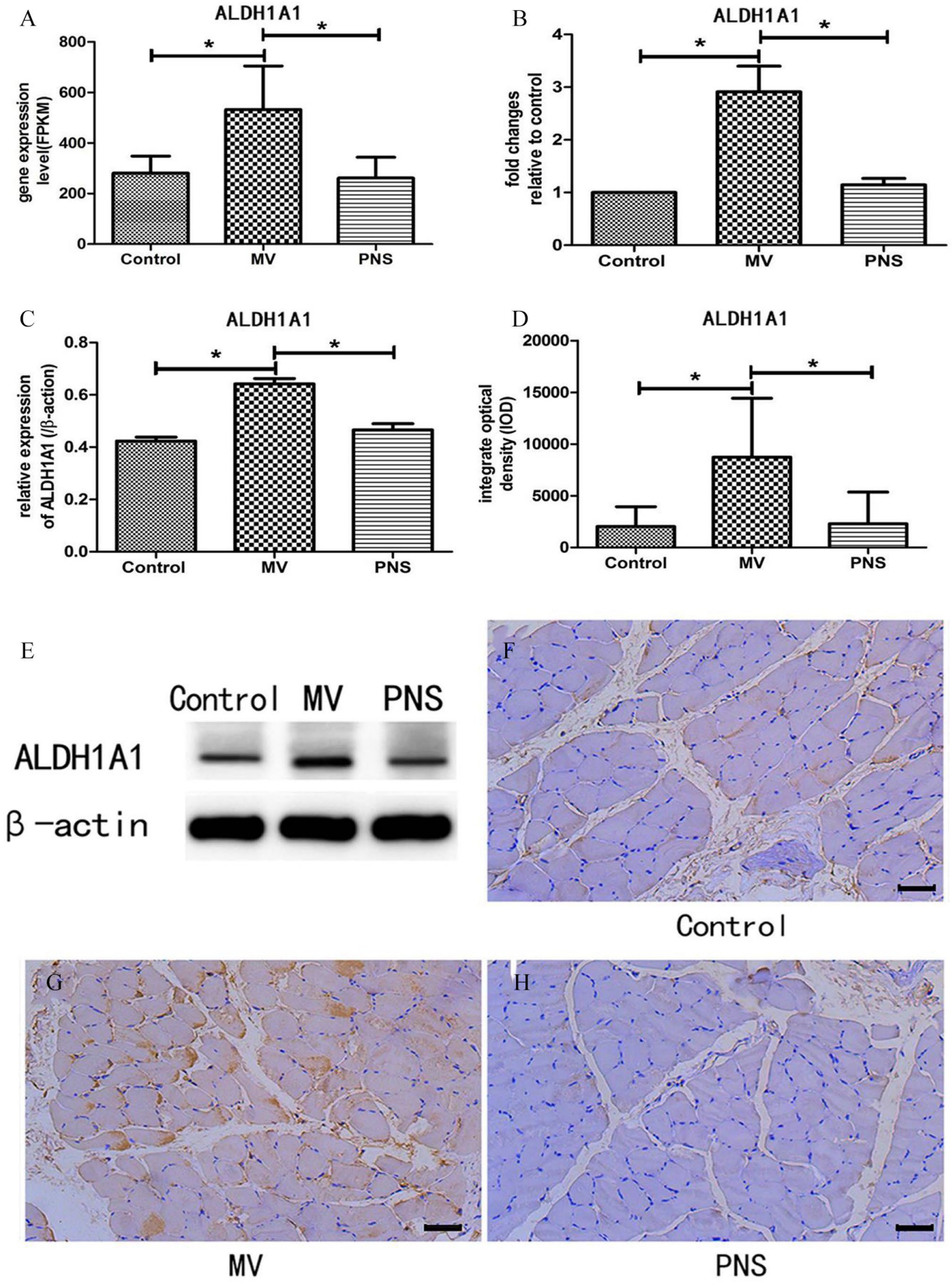

Figure 10. Downregulation of *Aldh1a1* mRNA expression and ALDH1A1 protein expression via electrically stimulated phrenic nerve particularly for mechanical ventilation. (A) RNA sequencing data. Mean ± SD. *$P < 0.05$. (B) RT-PCR data showing the fold-change in the *Aldh1a1* mRNA level relative to control. Mean ± SD. *$P < 0.05$. (C) Quantification of ALDH1A1 protein level by Western blotting. Mean ± SD. *$P < 0.05$. (D) Integral optical density (IOD) determined from immunohistochemistry experiments. Mean ± SD. *$P < 0.05$. (E) Representative image of Western blotting ($n = 6$ per group; for a given condition, running of all samples was undertaken on the same gel). (F to H) Representative images of diaphragmatic sections immunostained for ALDH1A1 protein. Scale bars = 50 μm. (A color version of this figure is available in the online journal.)

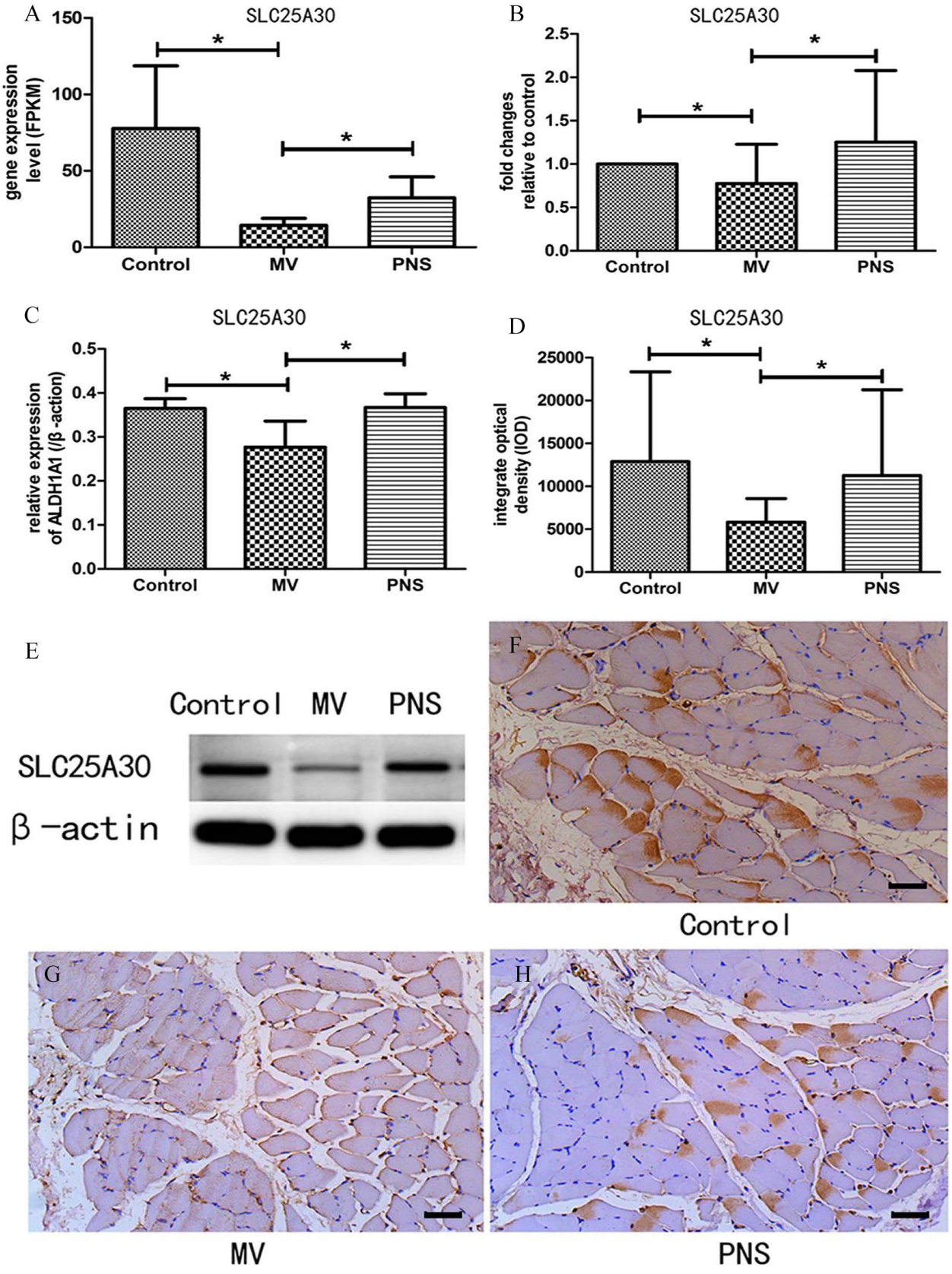

Figure 11. Upregulation of *Scl25a30* mRNA expression and SCL25A30 protein expression via electrically stimulated phrenic nerve particularly for mechanical ventilation. (A) RNA sequencing data. Mean ± SD. *$P < 0.05$. (B) RT-PCR data showing the fold-change in the *Scl25a30* mRNA level relative to control. Mean ± SD. *$P < 0.05$. (C) Quantification of SCL25A30 protein level by Western blotting. Mean ± SD. *$P < 0.05$. (D) Integral optical density (IOD) determined from immunohistochemistry experiments. Mean ± SD. *$P < 0.05$. (E) Representative image of Western blotting ($n = 6$ per group; for a given condition, running of all samples was undertaken on the same gel). (F to H) Representative images of diaphragmatic sections immunostained for SCL25A30. Scale bars = 50 μm. (A color version of this figure is available in the online journal.)

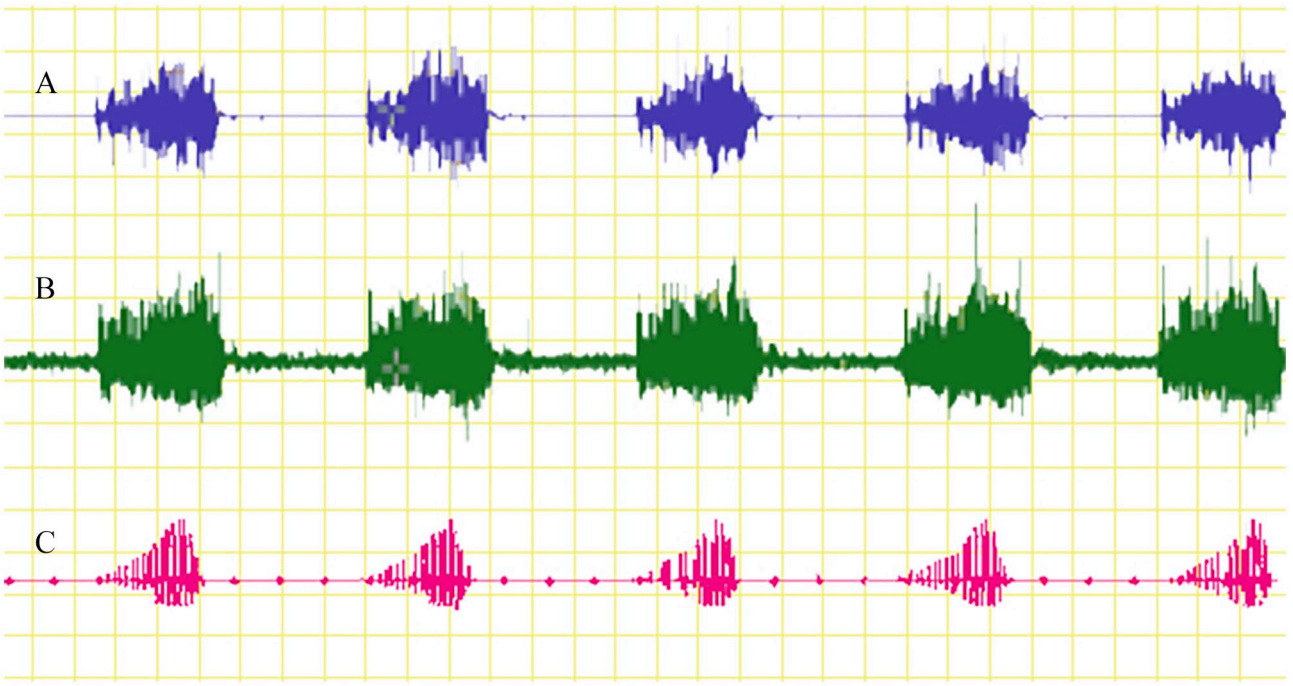

Figure 12. Comparison of (A) phrenic electromyography, (B) phrenic discharge, and (C) the simulated triangular electric current wave. (A color version of this figure is available in the online journal.)

The above observations indicate that diaphragmatic weakness during MV likely occurs within 12 h, which would be consistent with previous observations that VIDD develops after only 12 and 24 h in rats and rabbits, respectively.[23,28] Notably, scholars reported the association of the mechanisms underlying diaphragmatic injury and atrophy with oxidative stress, mitochondrial dysfunction and proteolysis.[29,30]

Diaphragmatic pacing has long been used in patients with high cervical spinal cord lesions and quadriplegia.[31] Previous studies confirmed the effects of diaphragmatic pacing on the improvement of diaphragmatic function, as well as its role in preventing and treating VIDD in critically ill patients.[32–34] The RESCUE2 study also demonstrated that temporary transvenous diaphragmatic pacing could correct diaphragmatic disuse atrophy and accelerate weaning in patients.[35] Although the RESCUE 2 study utilized a stimulation frequency of 15 Hz to provoke fused diaphragmatic contractions and mitigate against the development of VIDD, we believe that a frequency of 15 Hz may not optimally recruit fast-twitch type II myofibers and may not produce a sufficiently smooth contraction of diaphragmatic muscle. Currently, it is recommended that neurorehabilitation with electrical stimulation utilizes the minimum stimulus frequency that generates a fused muscle response.[36] However, no previous animal or human studies have determined the optimal PNS parameters, and in particular the optimal stimulation frequency, for potential mitigation against VIDD. Therefore, the present study used a stimulation frequency of 40 Hz, since this frequency recruits the type II fibers that are the first to atrophy following disuse. Of course, it is absolutely critical to avoid diaphragmatic fatigue and corresponding muscle damage when using high-frequency stimulation. Although fatigue was not evaluated in this study, we utilized specific approaches to minimize the risk of fatigue development. PNS-induced fatigue was minimized through the use of a triangular electric current wave (modulated in amplitude, with a progressive increase and a rapid decrease during the inspiratory period) that mimicked the physiological characteristics of normal phrenic nerve discharge (Figure 12). The above settings likely reduced the risk of high-frequency diaphragmatic fatigue.[37] However, it is essential to indicate the degree of diaphragmatic activation for the purpose of preventing VIDD. Therefore, additional research will be needed to determine the optimal frequency, dose, and duration of PNS for the prevention of VIDD in animal models as well as human patients.

A previous research reported the occurrence of MV-induced diaphragmatic atrophy originating from reduction of protein synthesis and elevation of proteolysis. Increased production of reactive oxygen species (ROS) could enhance muscle protein degradation via the ubiquitin proteasome system (UPS), and functioning in inactivity-induced atrophy in VIDD.[38] Attribution of protein loss to the upregulation of the UPS was recently figured out in an experimental study of endotoxin-induced diaphragmatic muscle dysfunction.[39] In line with published findings, the current research demonstrated that the UPS signaling pathway was significantly functionally upregulated during MV. Previous investigations have revealed that VIDD induces changes in gene expression that lead to energy oversupply relative to demand and diaphragmatic lipid accumulation during MV.[40] Contribution of lipid accumulation in skeletal muscle to oxidative stress and mitochondrial dysfunction was noted, enhancing the development of muscle atrophy. Our RNA-seq data indicated that the fatty acid degradation signaling pathway was activated in the PNS group compared with the MV group, raising the possibility that electrical stimulation protects the diaphragm by increasing diaphragmatic

contractile activity levels and reducing energetic substrate overload. However, the metabolic molecular mechanisms linking the UPS and fatty acid degradation signaling pathways to VIDD remain to be elucidated.

This study is the first to identify two key genes (*Aldh1a1* and *Slc25a30*) that are involved in VIDD and the mitigating effects of PNS. ROS are formed as normal products of oxygen metabolism in the cell, but their production can be increased under pathological conditions and cause damage. The imbalance between the antioxidant defense mechanism and ROS production results in oxidative stress leading to cellular damage. ALDH1A1 is one member of the acetaldehyde dehydrogenase (ALDH) superfamily that metabolizes endogenous and exogenous acetaldehyde to the corresponding carboxylic acids by producing NAD(P)H, thereby mitigating against oxidative stress, protecting the cell and supporting cellular homeostasis.[41] The level of ALDH1A1 is elevated by stress to protect against oxidative damage, and activation of ALDH1A1 may produce beneficial effects under specific disease or therapeutic conditions.[42] Our findings revealed the elevated expression of the *Aldh1a1* gene in the MV group versus that in the control and PNS groups, suggesting that this acted as a compensatory antioxidant mechanism to protect against the increased production of ROS in the diaphragm. Moreover, electrical stimulation (PNS) suppressed the enhancement of ALDH1A1 activity possibly through a reduction in oxidative stress. This raises the possibility that inhibition of ALDH1A1 may represent a new treatment for the prevention of VIDD. However, whether activation or inhibition of ALDH enzymes exerts beneficial effects depends on the specific conditions, necessitating a greater understanding of the role-played by ALDH1A1 in specific diseases.[43–46]

Solute carrier family-25 (SLC25) is a superfamily of transporters in the mitochondrial inner membrane in mammals, and SLC25 member-30 (SLC25A30) has been implicated in the regulation of ROS.[47] The *Slc25a30* gene encodes kidney mitochondrial carrier protein-1 (KMCP1), which transports sulfate and thiosulfate across the inner mitochondrial membrane and thereby modulates the level of the important gaseous signaling molecule, hydrogen sulfide (H_2S).[48] H_2S, in which its degradation rate and synthesis could be utilized to determine its cellular concentration, could protect cells against oxidative damage via directly scavenging ROS and activating cell signaling pathways that promote the expression of antioxidant enzymes.[49] Previous research has provided evidence that a H_2S donor can protect against VIDD, and it is possible that an exogenous H_2S donor supplements the endogenous levels of H_2S in diaphragmatic fibers during prolonged MV.[50] In view of the results of the present study, we propose that diaphragmatic H_2S synthesis was suppressed in the MV group due to the downregulation of *Slc25a30* and that PNS attenuated both the downregulation of *Slc25a30* and the decrease in H_2S synthesis to protect the diaphragmatic mitochondria against oxidative stress. Thus, PNS and its effects on two antioxidant genes (*Aldh1a1* and *Slc25a30*) may offer a new basis for the development of future therapies to prevent VIDD.

The limitations of the present research should be pointed out. First, this study had a small sample size and was limited to rabbits, so that, the generalizability of the findings to human patients or other animals remains unestablished. Second, CMV was performed for only 24 h, so that, the effects of PNS on VIDD during longer-duration CMV were not assessed. Third, systematic comparisons of different PNS regimens were not made. Fourth, it was not established whether the PNS-induced increase in SLC25A30 activity inhibited oxidative stress through an enhancement of H_2S synthesis. Further studies are required to establish the optimal PNS regimen for VIDD prevention and elucidate the detailed mechanisms through which the ALDH1A1 and SLC25A30 proteins contribute to the prevention of VIDD by PNS.

In conclusion, our study revealed that the onset of VIDD occurred rapidly (within 12 h) in rabbits undergoing MV. Furthermore, early initiation of intermittent electrical stimulation of the diaphragm during MV prevented the development of VIDD in rabbits. Notably, *Aldh1a1* and *Scl25a30* were identified as candidate genes involved in the prevention of VIDD by transvenous PNS. Our findings may help to identify new therapeutic strategies to prevent VIDD. The possible roles of ALDH1A1 and SCL25A30 protein levels as biomarkers for VIDD require further investigation.

AUTHORS' CONTRIBUTIONS

The participation of all the authors in different stages of the research is confirmed. DZ and XJL conducted the experiments. WYH developed the pulse generator used for phrenic nerve stimulation. PYH performed the bioinformatics analysis, and QN carried out the data processing and statistical analysis. DZ wrote the manuscript. The final manuscript was reviewed and approved by all the authors.

DECLARATION OF CONFLICTING INTERESTS

The author(s) declared no potential conflicts of interest with respect to the research, authorship, and/or publication of this article.

FUNDING

The author(s) disclosed receipt of the following financial support for the research, authorship, and/or publication of this article: The work was supported by General Program of Natural Science Foundation of Shanxi Province (grant number: 201901D111332).

ORCID ID

Dong Zhang https://orcid.org/0000-0001-7845-4289

REFERENCES

1. Walter JM, Corbridge TC, Singer BD. Invasive mechanical ventilation. *South Med J* 2018;**111**:746–53
2. Demoule A, Molinari N, Jung B, Prodanovic H, Chanques G, Matecki S, Mayaux J, Similowski T, Jaber S. Patterns of diaphragm function in critically ill patients receiving prolonged mechanical ventilation: a prospective longitudinal study. *Ann Intensive Care* 2016;**6**:75
3. Dres M, Dubé BP, Mayaux J, Delemazure J, Reuter D, Brochard L, Similowski T, Demoule A. Coexistence and impact of limb muscle and diaphragm weakness at time of liberation from mechanical ventilation in medical intensive care unit patients. *Am J Respir Crit Care Med* 2017;**195**:57–66
4. Liang F, Emeriaud G, Rassier DE, Shang D, Gusev E, Hussain SNA, Sage M, Crulli B, Fortin-Pellerin E, Praud JP, Petrof BJ. Mechanical

ventilation causes diaphragm dysfunction in newborn lambs. *Crit Care* 2019;**23**:123
5. Levine S, Nguyen T, Taylor N, Friscia ME, Budak MT, Rothenberg P, Zhu J, Sachdeva R, Sonnad S, Kaiser LR, Rubinstein NA, Powers SK, Shrager JB. Rapid disuse atrophy of diaphragm fibers in mechanically ventilated humans. *N Engl J Med* 2008;**358**:1327–35
6. Schepens T, Verbrugghe W, Dams K, Corthouts B, Parizel PM, Jorens PG. The course of diaphragm atrophy in ventilated patients assessed with ultrasound: a longitudinal cohort study. *Crit Care* 2015;**19**:422
7. Demoule A, Jung B, Prodanovic H, Molinari N, Chanques G, Coirault C, Matecki S, Duguet A, Similowski T, Jaber S. Diaphragm dysfunction on admission to the intensive care unit. Prevalence, risk factors, and prognostic impact-a prospective study. *Am J Respir Crit Care Med* 2013;**188**:213–9
8. Supinski GS, Morris PE, Dhar S, Callahan LA. Diaphragm dysfunction in critical illness. *Chest* 2018;**153**:1040–51
9. Roesthuis L, van der Hoeven H, Sinderby C, Frenzel T, Ottenheijm C, Brochard L, Doorduin J, Heunks L. Effects of levosimendan on respiratory muscle function in patients weaning from mechanical ventilation. *Intensive Care Med* 2019;**45**:1372–81
10. Vaporidi K. NAVA and PAV+ for lung and diaphragm protection. *Curr Opin Crit Care* 2020;**26**:41–6
11. Bissett BM, Leditschke IA, Neeman T, Boots R, Paratz J. Inspiratory muscle training to enhance recovery from mechanical ventilation: a randomised trial. *Thorax* 2016;**71**:812–9
12. Ponikowski P, Javaheri S, Michalkiewicz D, Bart BA, Czarnecka D, Jastrzebski M, Kusiak A, Augostini R, Jagielski D, Witkowski T, Khayat RN, Oldenburg O, Gutleben KJ, Bitter T, Karim R, Iber C, Hasan A, Hibler K, Germany R, Abraham WT. Transvenous phrenic nerve stimulation for the treatment of central sleep apnoea in heart failure. *Eur Heart J* 2012;**33**:889–94
13. Dridi H, Yehya M, Barsotti R, Reiken S, Angebault C, Jung B, Jaber S, Marks AR, Lacampagne A, Matecki S. Mitochondrial oxidative stress induces leaky ryanodine receptor during mechanical ventilation. *Free Radic Biol Med* 2020;**146**:383–91
14. Tang H, Shrager JB. The signaling network resulting in ventilator-induced diaphragm dysfunction. *Am J Respir Cell Mol Biol* 2018;**59**: 417–27
15. Smuder AJ, Sollanek KJ, Nelson WB, Min K, Talbert EE, Kavazis AN, Hudson MB, Sandri M, Szeto HH, Powers SK. Crosstalk between autophagy and oxidative stress regulates proteolysis in the diaphragm during mechanical ventilation. *Free Rad Biol Med* 2018;**115**:179–90
16. Shanely RA, Zergeroglu MA, Lennon SL, Sugiura T, Yimlamai T, Enns D, Belcastro A, Powers SK. Mechanical ventilation-induced diaphragmatic atrophy is associated with oxidative injury and increased proteolytic activity. *Am J Respir Crit Care Med* 2002;**166**:1369–74
17. Martin AD, Joseph AM, Beaver TM, Smith BK, Martin TD, Berg K, Hess PJ, Deoghare HV, Leeuwenburgh C. Effect of intermittent phrenic nerve stimulation during cardiothoracic surgery on mitochondrial respiration in the human diaphragm. *Crit Care Med* 2014;**42**:e152–16
18. Liu R, Li G, Ma H, Zhou X, Wang P, Zhao Y. Transcriptome profiling of the diaphragm in a controlled mechanical ventilation model reveals key genes involved in ventilator-induced diaphragmatic dysfunction. *BMC Genomics* 2021;**22**:472
19. Hrdlickova R, Toloue M, Tian B. RNA-Seq methods for transcriptome analysis. *WIREs RNA* 2017;**8**:e1364
20. Costa-Silva J, Domingues D, Lopes FM. RNA-Seq differential expression analysis: an extended review and a software tool. *PLoS ONE* 2017; **12**:e0190152
21. Langfelder P, Horvath S. WGCNA: an R package for weighted correlation network analysis. *BMC Bioinformatics* 2008;**9**:559
22. Bernard N, Matecki S, Py G, Lopez S, Mercier J, Capdevila X. Effects of prolonged mechanical ventilation on respiratory muscle ultrastructure and mitochondrial respiration in rabbits. *Intensive Care Med* 2003;**29**:111–8
23. Sassoon CS, Caiozzo VJ, Manka A, Sieck GC. Altered diaphragm contractile properties with controlled mechanical ventilation. *J Appl Physiol (1985)* 2002;**92**:2585–95
24. Capdevila X, Lopez S, Bernard N, Rabischong E, Ramonatxo M, Martinazzo G, Prefaut C. Effects of controlled mechanical ventilation on respiratory muscle contractile properties in rabbits. *Intensive Care Med* 2003;**29**:103–10
25. Jiang TX, Reid WD, Road JD. Delayed diaphragm injury and diaphragm force production. *Am J Respir Crit Care Med* 1998;**157**:736–42
26. Feldman AT, Wolfe D. Tissue processing and hematoxylin and eosin staining. *Methods Mol Biol* 2014;**1180**:31–43
27. Pillai-Kastoori L, Schutz-Geschwender AR, Harford JA. A systematic approach to quantitative Western blot analysis. *Anal Biochem* 2020;**593**: 113608
28. Powers SK, Shanely RA, Coombes JS, Koesterer TJ, McKenzie M, Van Gammeren D, Cicale M, Dodd SL. Mechanical ventilation results in progressive contractile dysfunction in the diaphragm. *J Appl Physiol (1985)* 2002;**92**:1851–8
29. Hyatt HW, Ozdemir M, Yoshihara T, Nguyen BL, Deminice R, Powers SK. Calpains play an essential role in mechanical ventilation-induced diaphragmatic weakness and mitochondrial dysfunction. *Redox Biol* 2021;**38**:101802
30. Powers SK, Hudson MB, Nelson WB, Talbert EE, Min K, Szeto HH, Kavazis AN, Smuder AJ. Mitochondria-targeted antioxidants protect against mechanical ventilation-induced diaphragm weakness. *Crit Care Med* 2011;**39**:1749–59
31. DiMarco AF. Diaphragm pacing. *Clin Chest Med* 2018;**39**:459–71
32. Keough-Delgado E, López-Rodríguez L, de Olaiz B, Bertomeu-García A, Peñuelas Jiménez-Fernández ÓM, Gato-Díaz P, Pérez-Domínguez H, Pérez-Vizcaíno F, Schultz MJ, Lorente JA. Case studies in physiology: physiological and clinical effects of temporary diaphragm pacing in two patients with ventilator-induced diaphragm dysfunction. *J Appl Physiol* 2021;**130**:1736–42
33. Yang M, Wang H, Han G, Chen L, Huang L, Jiang J, Li S. Phrenic nerve stimulation protects against mechanical ventilation-induced diaphragm dysfunction in rats. *Muscle Nerve* 2013;**48**:958–62
34. Reynolds SC, Meyyappan R, Thakkar V, Tran BD, Nolette MA, Sadarangani G, Sandoval RA, Bruulsema L, Hannigan B, Li JW, Rohrs E, Zurba J, Hoffer JA. Mitigation of ventilator-induced diaphragm atrophy by transvenous phrenic nerve stimulation. *Am J Respir Crit Care Med* 2017;**195**:339–48
35. Evans D, Shure D, Clark L, Criner GJ, Dres M, de Abreu MG, Laghi F, McDonagh D, Petrof B, Nelson T, Similowski T. Temporary transvenous diaphragm pacing vs. standard of care for weaning from mechanical ventilation: study protocol for a randomized trial. *Trials* 2019;**20**:60
36. Sheffler LR, Chae J. Neuromuscular electrical stimulation in neurorehabilitation. *Muscle Nerve* 2007;**35**:562–90
37. Jammes Y, Collett P, Lenoir P, Lama A, Berthelin F, Roussos C. Diaphragmatic fatigue produced by constant or modulated electric currents. *Muscle Nerve* 1991;**14**:27–34
38. Hooijman PE, Beishuizen A, Witt CC, de Waard MC, Girbes AR, Spoelstra-de Man AM, Niessen HW, Manders E, van Hees HW, van den Brom CE, Silderhuis V, Lawlor MW, Labeit S, Stienen GJ, Hartemink KJ, Paul MA, Heunks LM, Ottenheijm CA. Diaphragm muscle fiber weakness and ubiquitin-proteasome activation in critically ill patients. *Am J Respir Crit Care Med* 2015;**191**:1126–38
39. Haegens A, Schols AM, Gorissen SH, van Essen AL, Snepvangers F, Gray DA, Shoelson SE, Langen RC. NF-κB activation and polyubiquitin conjugation are required for pulmonary inflammation-induced diaphragm atrophy. *Am J Physiol Lung Cell Mol Physiol* 2012;**302**:L103–10
40. Picard M, Jung B, Liang F, Azuelos I, Hussain S, Goldberg P, Godin R, Danialou G, Chaturvedi R, Rygiel K, Matecki S, Jaber S, Des Rosiers C, Karpati G, Ferri L, Burelle Y, Turnbull DM, Taivassalo T, Petrof BJ. Mitochondrial dysfunction and lipid accumulation in the human diaphragm during mechanical ventilation. *Am J Respir Crit Care Med* 2012;**186**:1140–9
41. Etienne J, Joanne P, Catelain C, Riveron S, Bayer AC, Lafable J, Punzon I, Blot S, Agbulut O, Vilquin JT. Aldehyde dehydrogenases contribute to skeletal muscle homeostasis in healthy, aging, and Duchenne muscular dystrophy patients. *J Cachexia Sarcopenia Muscle* 2020;**11**:1047–69
42. Singh S, Brocker C, Koppaka V, Chen Y, Jackson BC, Matsumoto A, Thompson DC, Vasiliou V. Aldehyde dehydrogenases in cellular responses to oxidative/electrophilic stress. *Free Radic Biol Med* 2013; **56**:89–101

43. Calleja LF, Yoval-Sánchez B, Hernández-Esquivel L, Gallardo-Pérez JC, Sosa-Garrocho M, Marín-Hernández Á, Jasso-Chávez R, Macías-Silva M, Salud Rodríguez-Zavala J. Activation of ALDH1A1 by omeprazole reduces cell oxidative stress damage. *FEBS J* 2021;**288**:4064–80
44. Makia NL, Amunom I, Falkner KC, Conklin DJ, Surapureddi S, Goldstein JA, Prough RA. Activator protein-1 regulation of murine aldehyde dehydrogenase 1a1. *Mol Pharmacol* 2012;**82**:601–13
45. Koppaka V, Thompson DC, Chen Y, Ellermann M, Nicolaou KC, Juvonen RO, Petersen D, Deitrich RA, Hurley TD, Vasiliou V. Aldehyde dehydrogenase inhibitors: a comprehensive review of the pharmacology, mechanism of action, substrate specificity, and clinical application. *Pharmacol Rev* 2012;**64**:520–39
46. Li B, Yang K, Liang D, Jiang C, Ma Z. Discovery and development of selective aldehyde dehydrogenase 1A1 (ALDH1A1) inhibitors. *Eur J Med Chem* 2021;**209**:112940
47. Palmieri F, Monné M. Discoveries, metabolic roles and diseases of mitochondrial carriers: a review. *Biochim Biophys Acta* 2016;**1863**:2362–78
48. Gorgoglione R, Porcelli V, Santoro A, Daddabbo L, Vozza A, Monné M, Di Noia MA, Palmieri L, Fiermonte G, Palmieri F. The human uncoupling proteins 5 and 6 (UCP5/SLC25A14 and UCP6/SLC25A30) transport sulfur oxyanions, phosphate and dicarboxylates. *Biochim Biophys Acta* 2019;**1860**:724–33
49. Veeranki S, Tyagi SC. Role of hydrogen sulfide in skeletal muscle biology and metabolism. *Nitric Oxide* 2015;**46**:66–71
50. Ichinoseki-Sekine N, Smuder AJ, Morton AB, Hinkley JM, Mor Huertas A, Powers SK. Hydrogen sulfide donor protects against mechanical ventilation-induced atrophy and contractile dysfunction in the rat diaphragm. *Clin Transl Sci* 2021;**14**:2139–45

(Received November 9, 2021, Accepted February 15, 2022)